Facile Catalytic Combustion of Rice Husk and Burning Temperature Dependence of the Ashes

Liangming Xiong,*,† Edson H. Sekiya,† Shigetaka Wada,‡ and Kazuya Saito†

Frontier Materials Laboratory, Research Center for Advanced Photon Technology, Toyota Technological Institute, 2-12-1 Hisakata, Tempaku, Nagoya 468-8511, Japan, and Department of Materials Science, Chulalongkorn University, Bangkok 10330, Thailand

ABSTRACT In this work, it was discovered and demonstrated that the combustion of rice husk is a catalytic process by the thermoanalytical technique. The catalyst involves the oxides of such transition metals as Mn, Fe, and Cu, which are mainly formed in the initial stage of rice husk combustion and remain in the rice husk ash as an impurity. Mn^{2+} ions of various concentrations were reloaded into the HCl-washed husk for cocombustion. As a result, the complete combustion temperature of the husk was decreased exponentially depending on the Mn^{2+} concentration. By the facile Mn loading technique using a 0.5 M solution, the combustion temperature can be decreased by ~100 °C, and the resulting ashes themselves can be a good catalyst in the complete combustion of many other organic compounds. The physicochemical properties and amorphous structure of the ashes from both the raw and HCl-washed husks were found to be strongly dependent on the burning temperature. A decreased complete rice husk combustion temperature can be beneficial in preparing porous amorphous silica with high surface area, high densification, and small Si−O−Si band angles.

KEYWORDS: rice husk • catalytic combustion • manganese oxide • ash • burning temperature dependence

1. INTRODUCTION

According to the statistical data of Food and Agriculture Organization, the 2007 annual world paddy production is about 660 million tons (MTs) (1). Of a paddy, about 20 wt % is husk, so rice husk (RH) has an annual production of more than 130 MTs. Thus, RH is an abundantly available agricultural byproduct in rice-growing countries. RH can be regarded as an organic and inorganic composite biomaterial. The organic part is composed of cellulose, lignin, hemicellulose, and other organic compounds, which are only about 2% in mass (2, 3). The inorganic part is mainly silica, which is mostly concentrated in the outer epidermal cells, according to Park's observations (4). The rest include K^+, Na^+, Ca^{2+}, Mg^{2+}, Cl^-, and so on (2, 4). In general, much moisture is also adsorbed within RH. The chemical compositions of RH vary from sample to sample, strongly related to the type of paddy, crop year, climatic variation, geographical conditions, and even the fertilizers used in paddy growth (2, 3, 5). When RH is combusted in air, the combustibles can be mostly burned off and some solid products, only about 10−25% in mass of RH (2, 3, 6), are left. The solid products are named rice husk ash (RHA) and consist of ~90 wt % silica and many other oxides as the impurity (3, 6, 7). In general, RHA also has some carbon residues (2, 6), owing to incomplete combustion of the organics. The impurity oxides in RHA may just be formed in RH combustion, and before combustion, their precursors may be some salts or chelates according to Park's observations (4). When the precursors are combusted in air, they can be oxidized or replaced by oxygen. RHA is porous and possesses a high surface area (5), so it can also adsorb much moisture. Therefore, the solid combustion products should not be taken for granted as the inorganic part of RH, despite having been extensively adopted.

Traditionally, RH is widely used as feeding and bedding material for animals, a source of thermal energy, and a reinforcement material for making composite products like bricks. However, these traditional applications are of low profits, and in many cases, RH is discarded as agricultural waste, which is mostly burned in open heaps (8). That means not only big waste but also some environmental problems. Therefore, how to more efficiently utilize RH and the ashes becomes an issue and also a need. In the past decades, many efforts have been made to industrially utilize RH under controlled conditions and to utilize the ashes in a variety of value-added products (2, 9). For example, RH is used as fuel for calorific power (10), and RHAs are widely used as a raw material of high compressive-strength cementious materials (2, 9, 11), as a reinforcing agent of thermoplastics or filters of some polymers (2, 9, 12), as a starting material for the synthesis of zeolites and mesoporous silica (2, 9, 13), as a catalyst support (14), and as a host for ion or group adsorption (15).

Directly burning RH as received or as simply pretreated is the conventional technique to exploit the calorific value

* To whom correspondence should be addressed. E-mail: lmxiong@toyota-ti.ac.jp.
Received for review July 8, 2009 and accepted October 14, 2009
† Toyota Technological Institute.
‡ Chulalongkorn University.
DOI: 10.1021/am9004623

and to obtain silica for commercial use. This is very simple and facile but brings up some associated problems, such as an uncontrolled local temperature, incomplete combustion, a large emission of toxic gases, the formation of crystallites, and so on. From the viewpoint of burning RH in power plants, decreased temperatures for the complete combustion of RH are highly desired (10). A decreased combustion temperature can mitigate requirements for the thermochemical stability of furnace construction materials, reduce erosion of the apparatus, diminish heat losses through the apparatus wall, and improve the explosion safety of the heat-generating installations. The complete oxidation of the combustibles can reach heating output and exclude secondary reactions that form toxic products. From the viewpoint of application of RHA or rice husk silica (RHS), noncrystallization, high purity, high porosity, and high specific surface area (SSA) are highly desired (16). In a combination of both viewpoints, a controllable decrease in the complete combustion temperature should be necessary and beneficial in common. The utilization of a vibrofluidized bed of catalysts makes it possible to burn RH at decreased temperatures (10), but the millimetric catalyst particles are ill dispersed over the RH pieces, limiting the catalytic effect. Moreover, a large amount of the oxide impurities, in particular, K_2O and P_2O_5, still remain in the ashes. The production of K_2O as a flux can promote crystallization of the ashes (17); K_2O and P_2O_5 can react with the porous silica to form binary or ternary phases. This, in RH combustion, can result in a decreased SSA for the ashes and also some carbon residues in them (6, 17, 18). Acid treatment of RH before burning was widely employed to effectively solve such problems as oxide and carbon impurities in the ashes and the ready crystallization of the ashes (2, 6, 9, 16), but very few or no results showed that the pretreatments could bring down the complete combustion temperatures of RH. For the RH combustion in power plants, therefore, the pretreatment means only an increase in the cost. Until now, no way has been proposed to well meet the combined application requirements of both RH for power and RHA in high value-added fields. Such a way should be of particular interest in the highly efficient utilization of the abundant agricultural waste RH.

As for the acid-washing pretreatments, their effects on the thermal decomposition (19), thermal resolution (20), molecule structure (16) of the organics in RH, and, in particular, the mass loss behavior (16, 19−22) have been extensively investigated, but their influence on combustion reaction temperatures received only a small amount of attention (19). On the other hand, the properties and structure decide the use of RHA or RHS, so RHA or RHS has also been extensively studied in the properties and structure (5, 17, 22), but little attention was paid to whether and how the burning temperature (T_b) influences the properties and structure. A good understanding of the pretreatment influence on the RH combustion reaction temperatures, in particular on the terminal combustion temperature (T_{tc}), and a good understanding of the T_b influence behavior on the physicochemical properties and amorphous structure of RHA or RHS are very necessary not only for the industrial burning of RH but also for the applications of RHA.

In this work, we present the initial discovery of the catalytic combustion behavior of raw RH. By comparison of the combustion of the unwashed and HCl-washed RHs with thermogravimetry and differential thermal analysis (TG−DTA), T_{tc} of RH was found to be increased by ∼73 °C with the leaching out of the impurity ions by acid. On the basis of this discovery, transition-metal ions like Mn^{2+} were reloaded into the HCl-washed husk. As a result, T_{tc} of RH was decreased again, and the decreased degree strongly depends on the Mn^{2+} concentration. The manganese oxides (MnO_x, $x = 1$, 1.5, or 2) produced in the early-combustion stage of the Mn^{2+}-loaded RHs played the role of catalyst in the mid- and late-combustion stages. Following this route, T_{tc} of RH was decreased by over 100 °C, which is very profitable for the industrial burning of RH. Furthermore, the final ashes, supported by MnO_x, themselves can be used as a good catalyst in the oxidation of many organic compounds. The T_b dependence of the physicochemical properties and structure of the ashes was also investigated. The SSA, amorphous structure, Si−O−Si bond angle, and densification are all strongly dependent on T_b.

2. EXPERIMENTAL SECTION

2.1. Material Processing. RH was obtained from a local rice-milling plant. Some of the RH was directly burned as received. Some was thoroughly washed with flowing tap water for 24 h and then washed with distilled water three times with strong stirring. The water-washed husk was dried at 110 °C overnight. Next, 100 g of the dried husk was immersed in 2 L of a 1 M HCl solution and stirred for 1 h. The husk was filtered and washed with distilled water three times and finally dried at 110 °C overnight. The ash samples were obtained by burning the raw and HCl-washed RHs at 400, 500, 600, 700, 800, and 900 °C, respectively, for 2 h at a heating rate of 10 °C min^{-1}. The raw and HCl-washed RHs and their corresponding ashes are labeled as RRH, WRH, RRHA, and WRHA, respectively.

2.2. Mn Loading. In the catalysis experiment, 1 g of WRH was immersed in 100 mL of 0.01, 0.05, 0.1, and 0.5 M manganese(II) acetate [$Mn(AC)_2$] solutions, respectively, under strong stirring at room temperature (RT) for 1.5 h. Then, the Mn^{2+}-loaded husks were filtered and dried at RT. They are labeled as MRH-n, where n = I, II, III, and IV, standing for the previously indicated concentrations, respectively. Finally, they were kept for subsequent thermal analysis.

2.3. Characterization. The thermal analysis of the RH samples was performed on a Rigaku Thermo plus 2 TG−DTA TG 8120 analyzer by heating to 1150 °C at a rate of 10 °C min^{-1} in air and by using Al_2O_3 as the standard reference and using Pt pans as the sample and reference holders. The TG and DTA curves were recorded simultaneously when the temperature rose. The chemical compositions of the ashes were determined by X-ray fluorescence (XRF) spectroscopy on a Rigaku RIX-3100 XRF spectrometer using a Rh target. The physicochemical properties of the ashes were examined by the N_2 sorption technique, operating on a Micromiritics Tristar 3000 analyzer at 77.35 K. The Brunauer−Emmett−Teller (BET) theory was used to determine SSA. The wide-angle powder X-ray diffraction (XRD) patterns of the ashes were taken on a Rigaku RINT-2500 X-ray diffractometer with Mo Kα ($\lambda = 0.7093$ Å) radiation. The voltage and current applied to the X-ray tube were 50 kV and 300 mA, respectively. The step width was 0.02°, and the scanning speed was 1.2° min^{-1}. The Fourier transform infrared

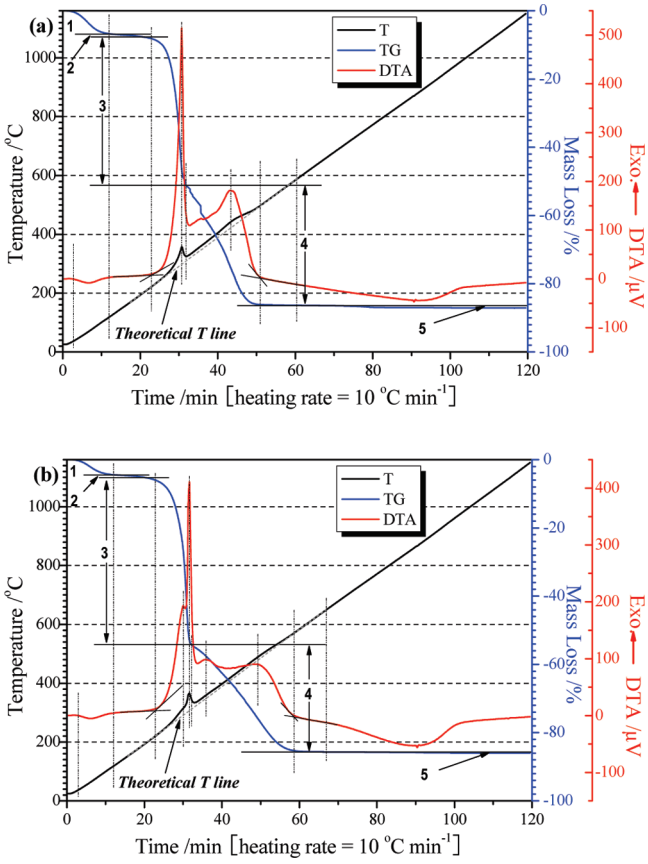

FIGURE 1. TG−DTA curves of RRH (a) and WRH (b).

(FT-IR) absorption spectrometry was performed on a Perkin-Elmer Multiscope FT-IR microscope. The spectrometry was taken in the IR reflection mode, in which the sample need not be mixed with any auxiliary chemical like KBr but pressed into a pellet directly with the ash powders.

3. RESULTS AND DISCUSSION

3.1. Combustion Behavior of RRH and WRH.

3.1.1. Thermal Process. Figure 1 shows the TG−DTA curves of RRH (a) and WRH (b). Both DTA curves are of a similar profile, in which an endothermic process occurs at the low-temperature stage and a broad and strong exothermic process occurs at the middle-temperature stage. Indicatively, having been corrupted from the strong exothermic process, the monitored temperature values of both samples much deviated from the theoretical line calculated following the heating rate, shown as the dashed line along the temperature curves in Figure 1. Thus, in the corrupted range, the temperature has an actual value and a theoretical value. The actual temperature is decided by both the theoretical value and the strong exotherm during combustion, while the latter is strongly related to the amount of combustibles, so the actual value is of higher uncertainty than the theoretical value. Thus, for a comparison of the characteristic temperatures between different samples, the use of the theoretical values seems more reasonable. Hereafter, the mentioned temperatures, if in the temperature range of the exothermic process, are referred to as the theoretical values in the theoretical temperature line. In the DTA curve of RRH (Figure 1a), the endothermic process occurred in 37−118 °C, and the strong exothermic process occurred in 220−498 °C. The exothermic process contains at least three exothermic peaks, at ∼298, ∼347, and ∼422 °C, respectively. The TG curve of RRH presents at least five mass loss stages, in the ranges of 37−118, 118−220, 220−309, 309−586, and over 586 °C, respectively. In the DTA curve of WRH (Figure 1b), the endothermic trough also occurred in 37−118 °C, and the strong exothermic process occurred in 219−571 °C. However, the exothermic process contains four clear exothermic peaks, at ∼292, ∼307, ∼349, and ∼479 °C, respectively. The TG curve of WRH can be also divided into at least five mass loss stages, in the ranges of 37−118, 118−219, 219 −312, 312−650, and over 650 °C, respectively. For a direct-viewing comparison, Table 1 lists the characteristic temperatures, temperature ranges, and mass losses for the different stages in the DTA and TG curves of RRH and WRH.

As introduced above, RH has various constituents, so the thermal process is very complex. It involves many different physical and chemical changes, which mainly include evaporation, volatilization, pyrolysis, oxidation, and replacement reaction. As we all know, evaporation and volatilization are endothermic processes and oxidation is an exothermic process. Taking into account that decomposition is an entropy increase process ($\Delta S > 0$), in thermodynamics, it can be deduced that the change of the enthalpy (ΔH) of a pyrolysis reaction is larger than 0. $\Delta H > 0$ means that pyrolysis of the organics in RH is an endothermic process. This was rarely correctly pointed out in the previous work (19, 23) on RH combustion. Replacement herein was not a strong process, owing to the very small amount of the impurity inorganic ions and groups. In DTA, therefore, the 37−118 °C endothermic trough is attributed to evaporation of the moisture from the husks. The broad exothermic process is predominantly due to oxidation of the organic constituents and their pyrolysis combustibles. Apart from the endothermic trough, no other endothermic peak was given below T_{tc}. Thus, pyrolysis, if it happens, must occur in the broad exothermic stage. When the temperature rose over T_{tc}, the DTA curves might vary with the further emission of some product gases, the probable eutectic reactions between the impurity oxides and RHS, and the crystallization process. In DTA, evidently, the combustion of both RHs was concentrated in the broad exothermic stage. In TG, the first stage is attributed to evaporation of the absorbed moisture; the second one may be due to the loss of the residual H_2O molecules or other molecules bonded to the wall surface of RHs; the third and fourth ones are attributed to the burnoff of the organics in RHs; the last one may be due to the emission of some residual gases or the gaseous products from the probable replacement reactions and the condensation of silanol groups. Therefore, in TG, combustion of both RHs mainly occurred in the third and fourth stages.

3.1.2. Combustion Reactions. Both DTA curves in Figure 1 show a few peaks. The multimodal profile is definitely related to not only the kinds of reactants but also the kinds of oxidation reactions. As one of the main organic

Table 1. Characteristic Temperature, Temperature Range, and Mass Loss for Different Stages in the DTA and TG Curves of RRH and WRH

	temperature range in DTA (°C)		temperature range (mass loss, %) in TG (°C)				
sample	endothermic	exothermic/peak temperature	stage 1	stage 2	stage 3	stage 4	stage 5
RRH	37−118	220−498/298, 347, 422	37−118 (6.9)	118−220 (0.8)	220−309 (43.5)	309−586 (35.2)	>586 (0.7)
WRH	37−118	219−571/292, 307, 349, 479	37−118 (4.4)	118−219 (0.7)	219−312 (48.9)	312−650 (31.6)	>650 (0.3)

constituents of RH, cellulose is a polysaccharide with the formula $(C_6H_{10}O_5)_n$ consisting of a linear chain of $\beta(1\rightarrow4)$-linked D-glucose units; hemicellulose is also a polysaccharide but consists of shorter and branched chains; lignin is a cross-linked racemic macromolecule with various monomers, like *p*-coumaryl alcohol, coniferyl alcohol, and sinapyl alcohol (24), which all consist of a benzene ring. Because of the difference in the bond energy or bond dissociation energy of the bonds C−O, C−C, and C−H, the CC bond of the benzene ring, and other bonds, the activation energies for their decomposition and oxidation are different. Accordingly, their decomposition and oxidation occur at different temperatures, accompanied by different ΔH values. The benzene ring generally is chemically more stable than the single bonds in the structure, so it would be decomposed and oxidized later than the single-bond parts. That is, lignin should be burned more slowly than cellulose and hemicellulose. Therefore, decomposition and oxidation of cellulose and hemicellulose are supposed to take place mainly in the early stage. Probably, the crossed linkages and the C−C chains of lignin can also be partially dissociated in this stage. As the temperature rises, the more stable parts of lignin become probable to be decomposed and oxidized. On the other hand, because the large emission of the volatile substances retards the transport of oxygen to lignin (10), not all of the more stable parts can be oxidized and many are carbonized. Thus, lignin is deduced to contribute mainly to the char faction, which was also supposed previously (23). In the late stage, the carbonaceous residues would interact with oxygen, which can proceed in various manners (10). Finally, some products like carbon monoxide are further oxidized, accompanied by a strong exotherm. In DTA in Figure 1, therefore, the strong exothermic peak in the early stage is mainly attributed to the oxidation of cellulose and hemicellulose or their pyrolysis products; the final exotherm is due to the oxidation of the carbonaceous products mainly originating from lignin. In TG, the third stage is mainly due to the burnoff of cellulose and hemicellulose, and the fourth stage is mainly due to the burnoff of lignin and the char fractions.

3.1.3. Catalytic Combustion Behavior. It should be noted that the end temperatures of the exothermic process of both RHs are different, ∼498 °C for RRH and ∼571 °C for WRH, as shown in Figure 1. The end temperature can be considered as T_{tc}. Thus, T_{tc} values of RRH and WRH are ∼498 and ∼571 °C, respectively. Evidently, as some constituents were leached out from RRH by acid washing, T_{tc} was increased by ∼73 °C. Therefore, compared with WRH combustion, RRH combustion is certainly a catalyzed process. In this sense, the out-leached constituents or their combustion derivatives played the role of a catalyst in RRH combustion. Besides T_{tc}, the final exothermic peak temperature (T_{fep}) was also much increased by leaching out some constituents from RRH. However, in the initial combustion stage, the onset combustion temperatures (T_{oc}) and the strongest exothermic peak temperatures (T_{sep}) varied little from RRH to WRH. This suggests that the catalyst should work mainly in the mid- and late-combustion stages instead of throughout the whole combustion process. To this, the probable cause is either that the catalyst already existed in RRH but did not promote the early-combustion reactions or that the catalyst itself did not exist in RRH before combustion but was just formed from their precursors in the initial combustion stage and worked in the subsequent stages.

Table 2. Chemical Compositions of RRHA and WRHA Obtained by Burning at 600 °C

		RRHA		WRHA	
comp.	spectr.	int. (kcps)	mass (%)	int. (kcps)	mass (%)
O	O Kα	0.1634	48.8368	0.1774	47.2601
Si	Si Kα	14.6877	26.8246	15.5882	27.9601
K	K Kα	2.1926	2.6343	0.0874	0.1075
Ca	Ca Kα	0.4149	0.6123	0.0413	0.0570
Mg	Mg Kα	0.1121	0.3253		
Mn	Mn Kα	0.1335	0.1913	0.0242	0.0311
P	P Kα	0.1378	0.1900	0.0884	0.1271
Cu	Cu Kα	0.4343	0.1599		
Na	Na Kα	0.0130	0.1044		
Al	Al Kα	0.0437	0.0854	0.0233	0.0442
Fe	Fe Kα	0.0682	0.0628	0.0406	0.0335
S	S Kα	0.0313	0.0478		

3.1.4. Potential Catalyst. The chemical compositions of the ashes RRHA and WRHA, obtained at 600 °C, which was proven high enough by the above TG−DTA results, were determined by XRF. Table 2 lists most of their compositions. Both have a high O content and a Si content, indicating that SiO_2 is their predominant component. The impurity compositions in RRHA include K, Ca, Mg, Mn, P, Cu, Na, Al, Fe, and so on. If they exist in the ash in the form of oxide, like K_2O, CaO, MgO, MnO_2, P_2O_5 (if instead of phosphates), CuO, Na_2O, Al_2O_3, and Fe_2O_3, respectively, the oxides can be calculated to be about 3.17, 0.86, 0.54, 0.3, 0.44, 0.2, 0.14, 0.16, and 0.09% in mass. After pretreatment by HCl washing of RRH, the contents of the impurity compositions in WRHA were much decreased. For example, the contents of K, Ca, Mn, P, Al, and Fe were decreased to about 0.11, 0.06, 0.03, 0.13, 0.04, and 0.03% in mass, respectively; the amounts of their corresponding oxides came to about 0.13, 0.08, 0.05, 0.29, 0.08, and 0.05% in mass, respectively. Except P, other impurities were mostly

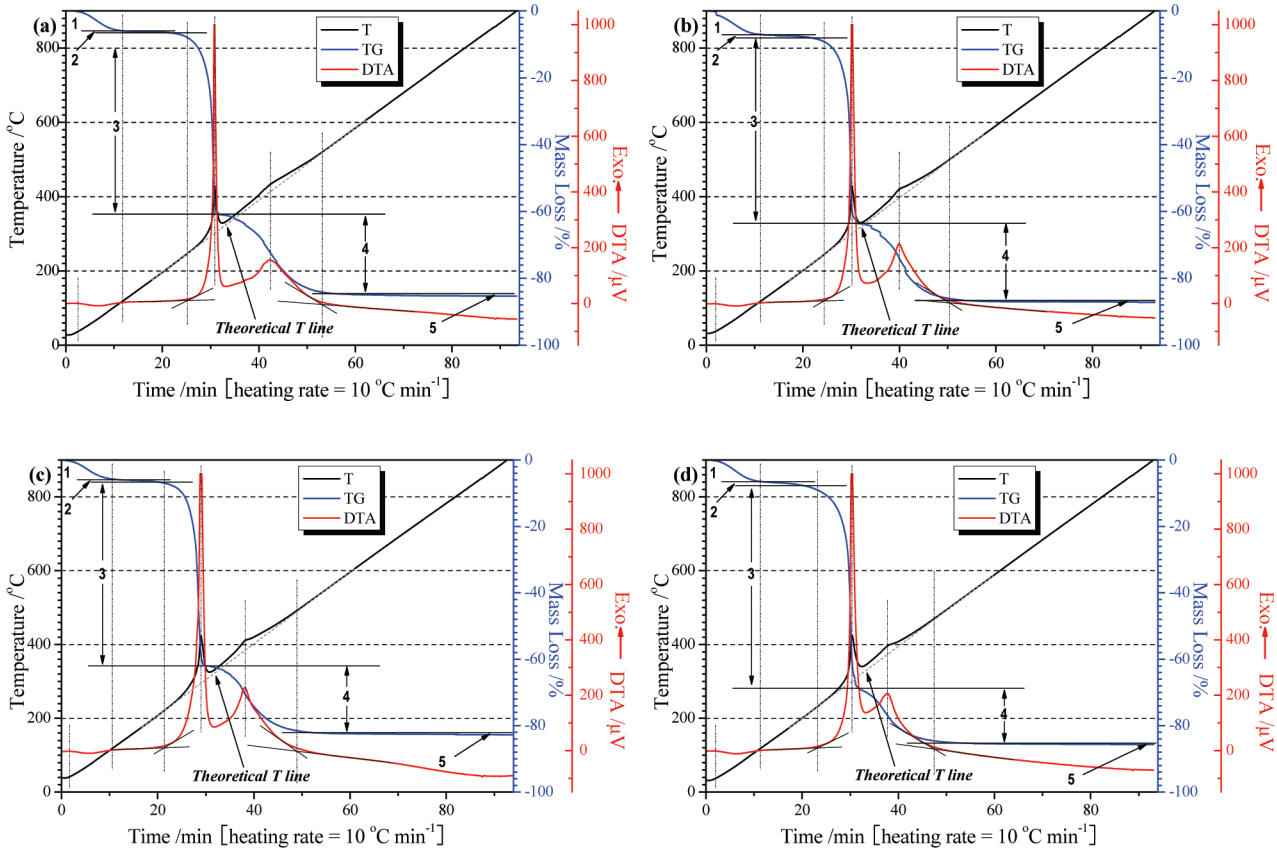

FIGURE 2. TG−DTA curves of the Mn-loaded WRHs: (a) MRH-I; (b) MRH-II; (c) MRH-III; (d) MRH-IV.

removed by pretreatment. Therefore, the potential catalyst ions may be those or some of those that were mostly removed by pretreatment. It is well-known that K_2O, CaO, MgO, and Na_2O cannot be used as the catalyst in the combustion or oxidation of organics. The P content was changed a little by pretreatment, and in general, its oxides are not an organic combustion or oxidation catalyst either. Nevertheless, the oxides of transition metals Mn, Cu, Mo, Fe, V, Co, Ni, and Zn are widely used as the catalysts in the complete oxidation of many organic compounds (25−29). Moreover, the contents of Mn, Cu, and Fe are also considerably high in RRHA and correspondingly high in RRH. Thus, they must belong to the catalyst components, or their oxides must be the potential catalyst in the RRH combustion. Many other researchers have also found that the ashes, obtained by burning different RHs as received, contain some transition-metal oxide impurities, and Fe_2O_3 and MnO_x generally are the main ones (5, 6, 17, 21). Therefore, their RRH combustion should also be a catalytic behavior.

3.2. Facile RH Catalytic Combustion Technique.

3.2.1. Demonstration of Catalytic Combustion Behavior. Taking into account the highest content of Mn among Mn, Cu, and Fe as the transition-metal impurities in RRHA and also taking into account the higher catalytic activity of MnO_x compared with Fe_2O_3 (25, 26), Mn^{2+} ions were chosen in this work for the demonstration experiment on the catalytic combustion.

Figure 2 shows the TG−DTA curves of MRH-*n*. In TG, the mass losses corresponding to the different stages are given in Table 3. The TG results will not be discussed any more herein because the loading of $Mn(AC)_2$ made the mass loss behavior more complex. In DTA, these heating processes are obviously similar. In particular, they all have two clear exothermic peaks, and the first one is the stronger one. Because of the strong exotherm from RH combustion and the additional exotherm from oxidation of the loaded $Mn(AC)_2$, the monitored actual temperatures during MRH-*n* combustion were disturbed a lot, but their theoretical T_{sep} values were all kept at ~300 °C, almost the same as those of RRH and WRH (shown in Figure 1). Interestingly, in the mid- and late-combustion stages, the theoretical T_{fep} and T_{tc} of MRH-*n* were both changed a lot as Mn^{2+} ions were reloaded within WRH. More importantly, they are all lower than those of the nonloaded WRH. For example, T_{fep} and T_{tc} of MRH-IV are 373 and 470 °C, respectively, while those of WRH are 479 and 571 °C, respectively. Both differences in T_{fep} and T_{tc} between the nonloaded WRH and the Mn-loaded WRH are over 100 °C. Undoubtedly, MRH-IV combustion was catalyzed by reloading Mn within WRH. Actu-

Table 3. Mass Loss for Different Stages in the TG Curves of MRH-I, -II, -III, and -IV

	mass loss for different stages in TG (%)				
sample	stage 1	stage 2	stage 3	stage 4	stage 5
MRH-I	4.6	0.5	42.1	18.4	0.6
MRH-II	5.5	0.7	43.1	17.9	0.4
MRH-III	4.6	0.6	42.9	15.6	0.4
MRH-IV	5.0	0.9	47.4	12.8	0.4

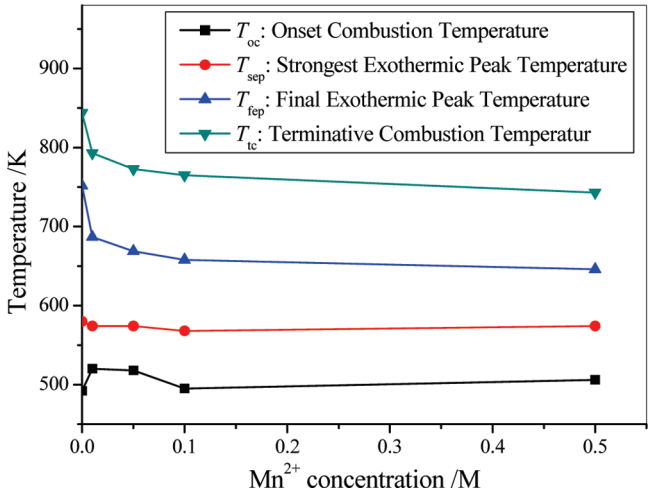

FIGURE 3. Relationship curves of the MRH-*n* combustion reaction temperature (K) versus the Mn^{2+} concentration.

ally, compared with RRH combustion, MRH-*n* combustion is more easily understood as a catalytic behavior because of the simplicity in the constituent change between MRH-*n* and WRH. In general, $Mn(AC)_2$ is not a combustion catalyst, but the oxides MnO_x are known to be excellent catalysts in the complete oxidation of many organic compounds, such as propane (26), acetone (27), ethanol (28), benzene (25), toluene (25, 28), and xylene (25). Therefore, the loaded $Mn(AC)_2$ cannot promote MRH-*n* combustion, but the combustion products MnO_x can, which, once formed, can catalyze the subsequent combustion process. As a result, the characteristic temperatures in the mid- and late-combustion stages were decreased. It is also evident that the combustion behavior of MRH-*n* resembles that of RRH more than that of WRH. Therefore, RRH combustion can be further confirmed to be a catalytic behavior. MnO_x operate as the catalyst mainly in two mechanisms: the suprafacial mechanism and the interfacial mechanism (28). The former is based on the interaction between the catalyst surface oxygen and reactants (10, 28) and is operative at low temperature (26, 28, 29), but RRH combustion at the low-temperature stage, i.e., the early stage, was not promoted, like MRH-*n* combustion. Therefore, it can be deduced that before combustion, the catalyst parts existed in RRH mainly in the form of precursors instead of as oxides like MnO_x, Fe_2O_3, and CuO. The catalyst oxides were just formed from the precursors in the early-combustion stage, subsequently played the catalyst role, and finally remained as oxide impurities in the ashes.

3.2.2. Mn Uptake Dependence of Combustion Temperatures. Figure 3 gives the relationship curves of T_{oc}, T_{sep}, T_{fep}, and T_{tc} (K) versus the Mn^{2+} concentration of the solution. Under the same solution impregnation conditions, the higher Mn^{2+} concentration of the solution means a higher Mn^{2+} uptake within WRH. In Figure 3, T_{oc} and T_{sep} irregularly vary around 493 and 573 K with the Mn^{2+} concentration. However, T_{fep} and T_{tc} decrease exponentially with increasing Mn^{2+} concentration, implying a strong Mn uptake dependence. Depending on the Mn uptake, the concentration of the reactant oxygen varies, further influencing the oxidation reactions involved in RH combustion. The rate of coke combustion depends on both the kinetic factors of the interaction of carbon with oxygen and carbon dioxide and the transport of oxygen to the surface of the burning carbon particles (10). Therefore, the presence and the increase of the catalyst oxides not only change the kinetic factors but also promote the transport of oxygen to the surface of the burning particles. A similar Mn uptake dependence was also reported in toluene combustion (28). This was supposed to be due to the fact that toluene combustion proceeded through the interfacial mechanism, associated with catalyst reducibility (28). Taking into account the similarity in the molecule structure between toluene and lignin, the interfacial mechanism can also be suitable in MRH-*n* combustion. At the beginning, Mn^{2+} ions are oxidized into higher valence states as MnO_x; subsequently, MnO_x are reduced, providing bulk oxygen available for oxidation of the combustibles. Besides the catalyst reducibility, certainly the increase of the surface oxygen of MnO_x can also promote combustion of RH in the initial stages (10, 28, 29). Therefore, after formation of the catalyst, both mechanisms can operate in the catalytic combustion of RH.

3.2.3. Interest in Industrially Burning RH. The exponential change tendency indicates that the catalyst performance can be increased by the Mn^{2+} uptake, but such temperatures as T_{fep} and T_{tc} cannot be increased limitlessly. Despite that, the Mn^{2+} loading technique is of particular importance in the burning of RH in power plants. The controlled decrease of T_{tc} allows mitigation of the burning apparatus requirements, diminishing of the heat losses through the apparatus, and improvement of the operation safety and life of the apparatus. On the other hand, Mn^{2+} ions are probably highly dispersed within RH via solution impregnation, and the produced MnO_x may be accordingly well dispersed over the host. Compared with the catalyst employed in the vibrofluizid bed (10), the well-dispersed MnO_x catalyst can operate more effectively on the complete combustion reactions, leading to fewer carbonaceous residues and less emission of some toxic products like carbon monoxide. For the industrial utilization of RH, of more practical interest is that, in order to decrease the complete combustion temperature, RRH can be directly employed to load Mn^{2+} ions via solution impregnation without being pretreated by acid, when one does not have to be concerned with the problem of the oxide impurities in the ash.

Figure 4 shows the DTA curve of a Mn-loaded RRH husk, which was prepared by directly soaking RRH into the 0.5 M ($Mn(AC)_2$ solution and then drying. Its T_{fep} (~380 °C) and T_{tc} (~460 °C) were found to be about 40 °C lower than those of RRH, respectively. Thus, the RRH catalytic combustion behavior can be enhanced by loading some additional Mn. That further suggests that the Mn loading within RRH by direct solution impregnation is also effective in decreasing the combustion temperature. This is very beneficial to the industrial burning of RRH.

3.3. Catalytic Combustion Effects on the Ashes.

3.3.1. On Morphology. Figure 5 shows the macromor-

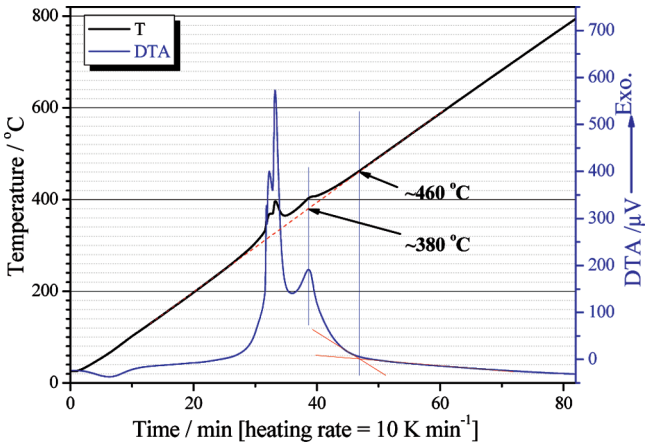

FIGURE 4. DTA curve of the Mn-loaded RRH using a 0.5 M solution.

FIGURE 5. Macromorphology of RRHA and WRHA obtained at various temperatures.

phology of RRHA and WRHA obtained at various T_b values at the same heating rate of 10 °C min^{-1} for 2 h. When both RHs were burned at 400−500 °C, in-color WRHA look darker than RRHA. This can be well explained by the catalytic combustion theory. The selected T_b is below T_{tc} of WRH (~571 °C), so WRH cannot be completely combusted, causing many carbonaceous residues in WRHA. However, RRH combustion can be promoted by the catalyst part, so more combustibles can be burned out, leading to the grayish-white ash RRHA with fewer carbon residues. As the catalytic combustion behavior of RRH was pointed out and demonstrated, some interesting experimental phenomena reported by others (6, 21) can be also well explained. For example, in ref 6, the HCl-treated RHA look blacker than the untreated RHA when they were obtained after calcining at 400 and 500 °C by slow heating. In ref 21, in DTA the exothermic process of the as-received husk was ended at the earliest, that of the sulfuric acid leached husk was ended subsequently, and that of the citric acid leached husk was ended at the latest. As T_b is increased over T_{tc} of WRH, WRHA look whiter than RRHA, and in RRHA some carbon black is still present even when T_b is up to 900 °C. To this, a generally recognized reason is the high content of the impurity alkali-metal oxides such as K_2O in RRHA (2, 6, 17). This may also be related to some other factors.

3.3.2. On Surface Area. Figure 6 shows SSAs of RRHA and WRHA, obtained at various T_b values. At the same T_b value, WRHA exhibits a much higher SSA than RRHA, more than twice of the latter's. For RRHA, SSA decreases

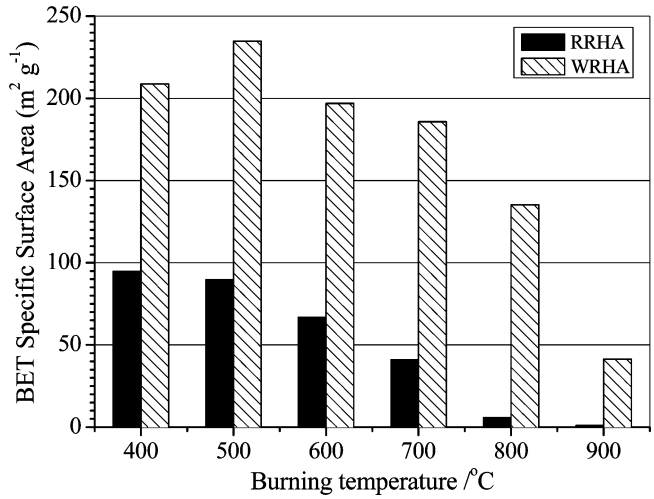

FIGURE 6. BET SSA of RRHA and WRHA obtained at various temperatures.

with an increase of T_b from 400 to 900 °C. When T_b was up to 800−900 °C, SSA of RRHA was sharply decreased. For WRHA, however, SSA at first increases with increasing T_b and then decreases step by step, and the highest one, ~235 m^2 g^{-1}, was obtained at 500 °C. Because the ashes obtained at 500 °C still contain many residual carbon particles in large sizes (clearly shown in Figure 5), a higher SSA is hopeful for WRHA if it is obtained at near T_{tc}. For porous silica with high SSA, there are many Si−OH groups on the framework (30). An increased T_b can destroy the metastable structure of its framework, causing SSA of the silica particles to be decreased. For WRHA, this may be the main mechanism regarding the T_b dependence of SSA. For RRHA, it may also take place, but at a high T_b, the main cause of the sharp decrease in SSA may be that some eutectic reactions occur between the porous silica and the oxide impurities like K_2O (6, 17, 18), CaO (18), P_2O_5 (if it truly exists as oxide instead of phosphates) (31), etc. (18). Actually, during RRH combustion, the local temperature of the burning particles was reported to be 100−300 °C higher than the furnace temperature (i.e., T_b) (10). The higher local temperature of the burning particles could also enhance both SSA decrease mechanisms in RRHA. Besides K_2O of a high content (2, 6, 17), the lower SSA and the rapid SSA decreases with T_b are another probable cause of the phenomenon that more carbon residues exist in RRHA. According to the anatomical observations on RH (4), SiO_2 is mostly located in the outer layer. In RH combustion, the large emission of volatile products retards the oxygen transfer to the inner layer, making the organics therein readily charred (10). A lower SSA of the burning particles can result in less oxygen reaching the carbonaceous substances in them. On the other hand, the catalyst quickens up the strong exothermic process, which further favors the eutectic reactions and the agglomeration of some particles. The agglomeration can make some char fractions isolated from oxygen and finally remain in RRHA. In experiment, the isolated carbon black is very difficult to fully remove by air annealing even at higher temperatures. For WRHA, the acid washing can remove most of the impurity ions and groups from RH,

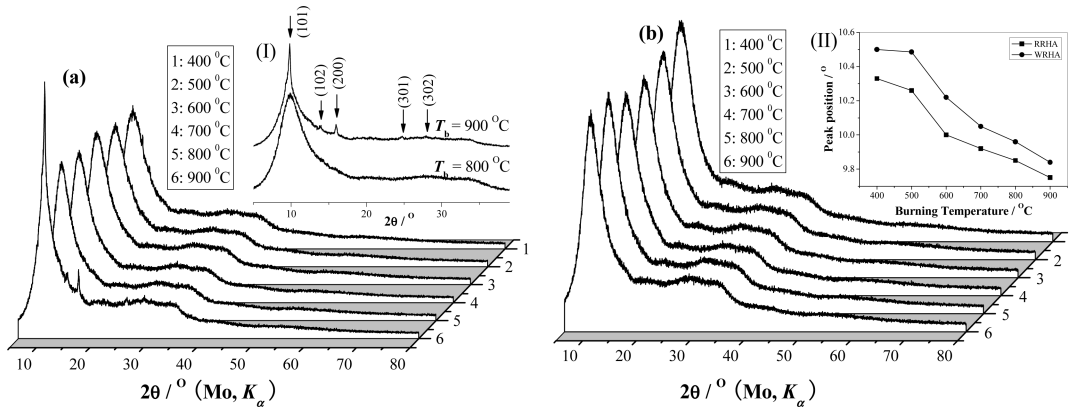

FIGURE 7. XRD patterns of RRHA (a) and WRHA (b) obtained at various temperatures. Insets: (I) enlarged patterns of RRHAs obtained at 800 and 900 °C, respectively, in part a; (II) burning temperature dependence of the strongest-diffraction-peak position of amorphous SiO_2 in RRHA and WRHA.

bringing down the possibility of low-temperature eutectic reactions. It can also lead to an increased SSA for the burning particles, implying that WRH and the burning particles are more accessible structures during combustion. The more accessible structure can favor more oxygen transfer to the char fractions, so that more of them can be burned out. In addition, the removal of catalyst ions by acid washing makes catalytic combustion impossible, so that the local temperature of the burning particles become impossible to increase so quickly. Thus, agglomeration of the solids can be slowed, which was also suggested by the slower SSA change of WRHA with T_b. More char fractions in the solids could be oxidized, and fewer or no carbon solids could remain in WRHA.

3.4. Burning Temperature Dependence on the Ashes. ***3.4.1. On the Physicochemical Property.*** As one of the representative physicochemical properties, SSA of the ashes was strongly related to the selected T_b values. Figure 6 also illustrates the T_b dependence of SSA, which has been discussed in section 3.3.2. A low but complete burning temperature can be beneficial to obtaining RHA with high SSA.

3.4.2. On the Short-Range-Order Structure. Figure 7 shows the XRD patterns of RRHA and WRHA, obtained at various T_b values. The one obtained from RRH at 900 °C clearly illustrates a few crystal diffraction peaks as well as the amorphous diffraction. This indicates that some crystal phase has been formed at 900 °C. The calculated *d* spacings of the crystal phase can well match those of the pattern collected in JCPDS card no. 82-0512, which is one of the standard patterns of cristobalite. That suggests that the detected crystal phase is cristobalite. The other patterns present only the amorphous diffraction. When the strongest amorphous SiO_2 peak position was compared, it was found that the 2θ value decreases with an increase of T_b (K), as shown in the inset II of Figure 7. The 2θ value is related to the short-range-order structure of the amorphous RHS, so its decrease in some sense implies the broadening of the short-range-order structure with T_b. That is, the densification of the amorphous structure is decreased with T_b. Furthermore, at the same T_b, the short-range-order diffraction of RRHA peaks at a smaller 2θ value than that of WRHA. That

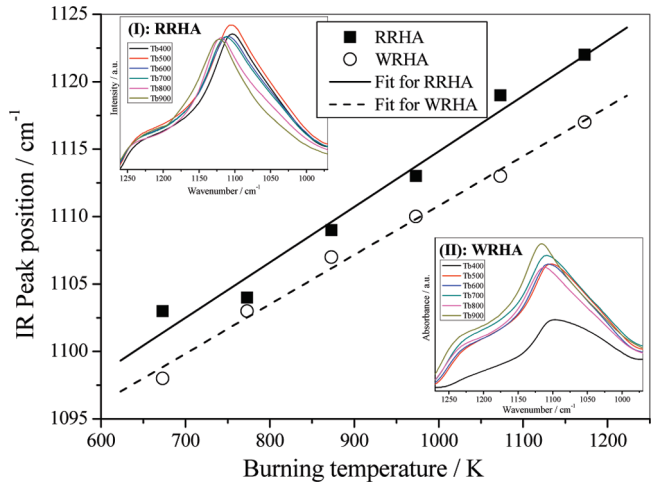

FIGURE 8. Burning temperature dependence of the IR stretching vibration absorption band of SiO_2 in RRHA and WRHA. Insets: IR absorption spectra of SiO_2 in RRHA (I) and WRHA (II).

also suggests that the densification of the amorphous SiO_2 structure of RRHA could be lower than that of WRHA.

3.4.3. On the Si−O−Si Bond Angle or Densification. In the IR absorption spectra of SiO_2, the band at ~1100 cm^{-1} is the most prominent and occurs with a prominent shoulder at ~1200 cm^{-1}. The band and shoulder are respectively the transverse- and longitudinal-optic components of the fundamental antisymmetric stretching vibration (32). This band has been directly correlated with the structure and various physical properties of SiO_2 glass (32). This band is also correlated with the Si−O−Si bond angle (33). The band has been found to shift to higher frequencies with an increase in the Si−O−Si bond angle (34). The band has also been observed to shift to lower frequencies with increasing densification (34−36). Figure 8 shows the change in the 1100 cm^{-1} IR absorption band of RRHA and WRHA versus T_b (K). The band of the RRHA group shifts to higher frequencies with increasing T_b, and so does the band of the WRHA group. At the same T_b, the band of RRHA peaks at a higher frequency, compared with that of WRHA. The change in the peak positions should reflect a change in the structure of SiO_2 due to a change in T_b or the acid-washing pretreatment. According to the previous observations (34−36), the T_b

dependence of the IR peak position suggests that, with increasing T_b in 673−1173 K, the Si−O−Si bond angle of RRHA and WRHA increases or the densification decreases. This is well-agreeable with the XRD result. The higher IR peak position of RRHA also suggests that the Si−O−Si bond angle of SiO_2 in RRHA is larger or the densification is lower compared with those of WRHA. This is also in good agreement with the XRD result. A generic line is constructed using a linear regression fit to all of the data points. The equations for the RRHA and WRHA lines in Figure 8 are respectively

$$\nu_{p-r} = (1073.692 \pm 2.99) + (0.041 \pm 0.003)T_b \quad (1)$$

and

$$\nu_{p-w} = (1074.245 \pm 1.564) + (0.037 \pm 0.002)T_b \quad (2)$$

where ν_i (cm^{-1}) is the peak position of the respective bands of RRHA and WRHA and T_b (K) is the burning temperature. Taking into account the measurement and fit errors, both lines can be considered parallel with the same slope, implying that T_b influences the structures of RRHA and WRHA in the same mechanism. The as-received burning temperature of RRHA or WRHA can be determined from eq 1 or 2 by simply measuring the peak positions of the ash.

3.5. Interest of RH Catalytic Combustion in RHA Applications. According to the above Results and Discussion, T_{tc} of RH combustion is highly controllable by the Mn uptake; the physicochemical properties, amorphous structure, and densification of RHA are strongly dependent on T_b. When T_b is set as T_{tc}, the obtained RHA will become also easily controlled by the Mn uptake in such structure and properties. It can be deduced that if T_{tc}, i.e., the complete combustion temperature, of WRH is decreased, the ash obtained at T_{tc} can be not only of a low carbon impurity but also of increased SSA. This is very beneficial to the application of the ashes in catalysis, adsorption, and chemical reaction as a starting material. Moreover, by burning RH at a decreased T_{tc}, the obtained RHA can be of higher densification and smaller Si−O−Si band angles, which may be of special interest in some fields. Therefore, the RH catalytic combustion technique by reloading Mn via solution impregnation is also of particular interest for the efficient applications of RHA. Furthermore, because of the excellent catalyst performance of the MnO_x guest, which may be well-dispersed over the RHA host, and because of the high SSA and the abundant acidic Si−OH groups of the RHA host, the final MnO_x-supported RHA obtained at a decreased T_{tc} may find direct use as a catalyst in the complete combustion and oxidation of many other organics (37). Besides Mn, many other transition-metal elements (e.g., Fe, Ni, Cu, etc.) can also be available for this facile catalytic combustion technique, and the resulting ashes can directly find different catalyst applications.

4. CONCLUSIONS

The combustion of raw RH was discovered and experimentally demonstrated to be a catalytic behavior. The catalyst is the transition-metal oxides whose precursors can be mostly leached out from the raw husk by pretreatment. On the basis of this discovery, we proposed a facile catalytic combustion technique in which Mn^{2+} ions of various concentrations were reloaded into the HCl-washed husk via solution impregnation. As a result, the complete cocombustion temperature of the Mn^{2+}-loaded husk can be decreased by over 100 °C, strongly depending on the Mn uptake. The physicochemical properties and structure of the ashes are strongly dependent on the burning temperature. As the burning temperature was increased, the SSA was decreased, and the Si−O−Si bond angle was increased or the densification was decreased. Therefore, this catalytic combustion technique is of importance not only in controllably decreasing the complete combustion temperature of RH but also in fabricating high value-added solid products with a low carbon impurity, high surface areas, controllable physicochemical properties and structure, and an excellent catalytic performance. Such a technique should be of particular profit to the industrial applications of both RH and the ash and be generalized by selecting many other transition-metal ions. Indeed, this work can be of much practical interest for the rice-growing countries.

Acknowledgment. We thank Prof. Y. Ohishi and A/P T. Suzuki for thermal analysis and are also grateful to Prof. J. Shi and A/P L. Zhang of SICCAS for the N_2 sorption experiment. This work was financially supported by the "High-Tech Research Center" project for private universities from MEXT of Japan.

REFERENCES AND NOTES

(1) Food and Agricultural commodities production. http://faostat.fao.org/site/339/default.aspx.
(2) Chandrasekhar, S.; Satyanarayana, K. G.; Pramada, P. N.; Raghavan, P.; Gupta, T. N. *J. Mater. Sci.* **2003**, *38*, 3159.
(3) Markovska, I. G.; Lyubchev, L. A. *J. Therm. Anal. Calorim.* **2007**, *89*, 809.
(4) Park, B.-D.; Wi, S. G.; Lee, K. H.; Singh, A. P.; Yoon, T.-H.; Kim, Y. S. *Biomass Bioenerg.* **2003**, *25*, 319.
(5) Liou, T.-H. *Carbon* **2004**, *42*, 785.
(6) Krishnarao, R. V.; Subrahmanyam, J.; Kumar, T. J. *J. Eur. Ceram. Soc.* **2001**, *21*, 99.
(7) Lanning, F. C. *J. Agric. Food Chem.* **1963**, *11*, 435.
(8) Sharma, A.; Rao, T. R. *Biores. Technol.* **1999**, *67*, 53.
(9) Sun, L.; Gong, K. *Ind. Eng. Chem. Eng.* **2001**, *40*, 5861.
(10) Simonov, A. D.; Mishenko, T. I.; Yazykov, N. A.; Parmon, V. N. *Chem. Sustainable Dev.* **2003**, *11*, 277.
(11) Ismail, M. S.; Waliuddin, A. M. *Constr. Build. Mater.* **1996**, *10*, 521.
(12) Chaudhary, D. S.; Jollands, M. C.; Cser, F. *Silicon Chem.* **2002**, *1*, 281.
(13) Rawtani, A. V.; Rao, M. S.; Gokhale, K. V. G. K. *Ind. Eng. Chem. Res.* **1989**, *28*, 1411.
(14) Ahmed, A. E.; Adam, F. *Microporous Mesoporous Mater.* **2007**, *103*, 284.
(15) Feng, Q.; Lin, Q.; Gong, F.; Sugita, S.; Shoya, M. *J. Colloid Interface Sci.* **2004**, *278*, 1.
(16) Umeda, J.; Kondoh, K.; Michiura, Y. *Mater. Trans.* **2007**, *48*, 3095.
(17) Shinohara, Y.; Kohyama, N. *Ind. Health* **2004**, *42*, 277.
(18) Armesto, L.; Bahillo, A.; Veijonen, K.; Cabanillas, A.; Otero, J. *Biomass Bioenerg.* **2002**, *23*, 171.
(19) Chakraverty, A.; Mishra, P.; Banerjee, H. D. *Thermochim. Acta* **1985**, *94*, 267.
(20) Rahman, I. A.; Ismail, J.; Osman, H. *J. Mater. Chem.* **1997**, *7*, 1505.

(21) Umeda, J.; Kondoh, K. *J. Mater. Sci.* **2008**, *43*, 7084.
(22) Genieva, S. D.; Turmanova, S. Ch.; Dimitrova, A. S.; Vlaev, L. T. *J. Therm. Anal. Calorim.* **2008**, *93*, 387.
(23) James, J.; Rao, M. S. *Thermochim. Acta* **1986**, *97*, 329, and references cited therein.
(24) Freudenberg, K.; Nash, A. C. *Constitution and Biosynthesis of Lignin*; Springer-Verlag: Berlin, 1968.
(25) Kim, S. C. *J. Hazard. Mater.* **2002**, *91*, 285.
(26) Baldi, M.; Escribano, V. S.; Amores, J. M. G.; Milella, F.; Busca, G. *Appl. Catal., B* **1998**, *17*, L175.
(27) Reed, C.; Lee, Y.-K.; Oyama, S. T. *J. Phys. Chem. B* **2006**, *110*, 4207.
(28) Aguero, F. N.; Scian, A.; Barbero, B. P.; Cadús, L. E. *Catal. Lett.* **2009**, *128*, 268.
(29) Mishra, T.; Mohapatra, P.; Parida, K. M. *Appl. Catal., B* **2008**, *79*, 279.
(30) Xiong, L.; Shi, J.; Gu, J.; Li, L.; Shen, W.; Hua, Z. *Solid State Sci.* **2004**, *6*, 1341.
(31) Balk, P.; Eldridge, J. M. *Proc. IEEE* **1969**, *57*, 1585.
(32) Agarwal, A.; Davis, K. M.; Tomozawa, M. *J. Non-Cryst. Solids* **1995**, *185*, 191, and references cited therein.
(33) Galeener, F. L. *Phys. Rev. B* **1979**, *19*, 4292.
(34) Devine, R. A. B. *J. Non-Cryst. Solids* **1993**, *152*, 50.
(35) Mackenzie, J. D. *J. Am. Ceram. Soc.* **1963**, *46*, 461.
(36) Arndt, J.; Stoffler, D. *Phys. Chem. Glasses* **1969**, *10*, 117.
(37) Larsson, P.-O.; Berggren, H.; Andersson, A.; Augustsson, O. *Catal. Today* **1997**, *35*, 137.

AM9004623